https://doi.org/10.1149/1945-7111/ac6a15

Suite of high-throughput experiments for screening solid electrolytes for Li batteries

Antranik Jonderian, Ethan Anderson, Rui Peng, Pengfei Xu, Shipeng Xia, Victor Cozea and Eric McCalla*

Department of Chemistry, McGill University, Montreal, Canada

* Corresponding author: eric.mccalla@mcgill.ca

Abstract: All-solid lithium batteries are an important technology to develop to achieve safer batteries with potentially longer life. Efforts over the past decade have generated a vast list of candidate solid electrolytes. High-throughput methods have already been useful in this context, but studies have been limited to room temperature ionic conductivities. Although a high ionic conductivity is necessary, this single property is insufficient to ensure function in a solid battery. Herein, a suite of high-throughput methods is introduced where 64 samples are synthesized simultaneously. Herein, we demonstrate for the first time the high-throughput capability of obtaining: (1) ionic conductivities at and above room temperature to extract activation energies, (2) electronic conductivities to evaluate the risk of dendrite growth within pellets, (3) electrochemical stability window, and (4) chemical stability against lithium. Importantly, the stability window is obtained by testing the electrolyte in a composite electrode with conductive carbon, thereby avoiding the overestimations of stability that are rampant in the literature. Each method was validated using two reference materials chosen as they show high contrast for all properties. The results systematically show excellent reproducibility and good agreement with the literature. This suite of techniques provides meaningful properties necessary to evaluate candidate solid electrolytes.

Introduction:

There is a global demand for safer and longer lasting energy storage devices for electric vehicles and grid energy due to the increasing reliance on intermittent renewable energy sources. Solid-state electrolyte based batteries are promising for fulfilling this demand. Commercial lithium-ion batteries are reaching their limits since important issues such as the flammable organic liquid electrolytes and limited electrochemical stability windows continue to limit their performance. Moreover, the liquid electrolyte cannot inhibit dendrite formation at fast-charging rates nor permit the use of lithium metal anodes. In contrast, solid electrolytes (SE) are inflammable and can potentially prevent dendrite formation thus they are considered a promising alternative. Over the past decades, a great deal of research has taken place to obtain solid electrolytes with the highest possible room temperature (RT) ionic conductivity. Indeed, the RT ionic conductivity and activation energy are essential properties to measure as SE with high ionic conductivity and low activation energy is needed to ensure minimal resistance at a wide temperature range. The total ionic conductivity is measured by electrochemical impedance spectroscopy (EIS) on a symmetric cell with two ion-blocking contacts. A few reports have performed these measurements in high-throughput.[1, 2]

However, there are a number of other key properties that must also be fulfilled for a solid electrolyte to be suitable for integration into a full battery.[3] The electronic conductivity, which is not frequently assessed, was shown to be correlated with dendrite formation from the bulk of the SE, with the smallest conductivity giving rise to dendrites being 2.2×10^{-9} S cm^{-1} at room temperature.[4] In the few cases where this property has been reported, DC polarization is used to measure electronic conductivity from the steady-state current. To date, no high-throughput paper has included this measurement. Similarly, solid electrolytes must have a suitable electrochemical

stability window (ESW) to enable the use of the anode at low potentials and the desired cathode at high potentials. Recently, it has become abundantly evident that the ESW is overestimated when measured on a Li/SE/Au cell configuration due to the poor electronic conductivity of the SE shutting down the parasitic reactions.[3, 5] Despite this well known error from this method, this approach continues to be utilized in the literature, and this leads to confusion and a lack of attention to the true limits of the materials under study. Obtaining a meaningful result for the stability window requires preparing the solid electrolyte as a working electrode by mixing it with a conductive additive to overcome the poor electronic conductivity of the material.[5-9] To date, very few studies have used this approach and no high-throughput studies have been performed with a suitable method to determine the ESW.

It is also important to note that metallic lithium continues to be an extremely interesting anode given its very high capacities. A solid electrolyte can potentially be used with lithium anodes while its high bulk modulus can prevent dendrite growth from the surface of the lithium. Therefore, it is imperative to investigate the stability of the solid electrolytes against lithium metal. The metallic lithium compatibility is typically investigated by measuring the evolution of the impedance using EIS after bringing the SE in contact with lithium metal.[10]

The conventional method of screening solid electrolytes one composition at a time, coupled with an incomplete suite of property measurements, has slowed down the development of SEs. Consequently, there is a need for high-throughput synthesis and characterization tools for exploring a wide range of composition spaces and the effect of broad substitutions into promising but limited materials. The high-throughput characterization tools should include screening the essential properties mentioned above as illustrated in Fig. 1, with the resulting radar plots helping to shortlist promising SEs for additional tests such as compatibility tests with specific cathodes

and full cell performance. The high-throughput tools will therefore help elucidate the structure-property relationships guiding the design of new materials. A previous report for high-throughput synthesis and characterization of solid electrolytes was done on thin films, and only structure and ionic conductivity were determined.[1] Previously, we have used the citrate sol-gel method as a versatile synthesis route to produce a variety of ceramics of high interest for battery materials.[2, 11-13] The characterization of solid electrolytes in our previous work was limited to room temperature ionic conductivities. Thus, herein, we developed high-throughput tools for screening solid-state electrolytes. We validated our setups by studying two model solid electrolytes: perovskite Li23-La27-Ti50 and garnet $Li_7La_3Zr_2O_{12}$. These two materials were chosen for their contrasting properties for the tests performed here. We optimized the citrate sol-gel method for synthesizing 64 samples and measured the key properties required for a good solid electrolyte using our developed high-throughput characterization tools, as illustrated in Fig. 1.

Experimental methods:

The various steps in Fig. 2 illustrate the methods used throughout. This demonstrates the typical workflow in our high-throughput studies of SEs. The solid electrolytes were synthesized by the citrate sol-gel method described in detail in ref. [13]. Solutions were prepared from the starting reagents in DI or ethanol (Ti only). Two materials were made for the proof-of-concept herein: lithium lanthanum titanate (LLTO) and undoped tetragonal lithium lanthanum zirconate (LLZO). These two materials were selected for their contrast in properties (e.g. the undoped LLZO has a low ionic conductivity while the LLTO show a much higher conductivity as per refs. [24-25]) such that a high-throughput suite of methods must be able to obtain precise measures for both these materials in order to be useful in developing new materials that could start with poor properties

and be improved with doping and/or changing synthesis conditions. For the synthesis of LLTO, first citric acid (4 M) was pipetted followed by the addition of $Ti(OCH_2CH_2CH_2CH_3)_4$ (98+% Acros Organics) (2M EtOH), $La(NO_3)_3$ (99.9% Alfa Aesar) (2M) and lastly $LiNO_3$ (99% Alfa Aesar) (2M) in mole percentages of 13/15/29/43 for Li/La/Ti/citric. For the synthesis of LLZO we used $LiNO_3$, $La(NO_3)_3$, and $Zr(OH)_2(OAc)_2$ (Sigma Aldrich) in a mole ratio of 7/3/2 respectively, followed by the addition of citric acid (4M) for a total cations to citric ratio of 1:0.75. The bulk content of the solvent was dried by heating at 80 °C for 12 hours after placing a smokestack above the cups to prevent cross-contamination during the heat treatments. After the powders were calcinated at 600 °C for 6 hours, green pellets were prepared in a homemade high-throughput pellet die (1 GPa maximum pressure). The LLTO pellets were sintered at 1200 °C for 6 hours while the LLZO were sintered at 900 °C for 3 hours. The surface of the sintered pellets was sanded with diamond sanding paper (800 grit). To determine reproducibility and precision, 64 LLTO pellets of identical composition were made herein. Furthermore, to demonstrate the contrast between materials for each characterization method, a few LLZO samples were also synthesized in the same high-throughput method.

Gold contacts were sputtered on the two faces of the polished pellets for the EIS and DC polarization measurements using the high-throughput cell described in refs. [13]. A Biologic SP150 potentiostat coupled with a Pickering multiplexer was used to measure the electrical response from 1MHz to 1Hz at 100 mV at RT and 50 °C to determine the activation energy from the Arrhenius plot. Prior to the 50 °C measurement, the cell was allowed to stabilize for 12 h (the high-throughput cell has a large thermal mass), such that the total measurement time is approximately 16 h (2 h per EIS for 64 samples, and 12 h stabilization). The EIS spectra were analyzed using the Z-fit tool of EC-Lab software in batch mode. The DC polarization measurements were done using a Keithley

213 quad voltage source with Keithley 2750 multimeter (the same high-throughput pseudo-potentiostat as used to do cyclic voltammetry for cathodes in refs. [13, 14]). However, to get the precision required, high resistance and high precision (10 kΩ) resistors were used to measure small currents through the pellets. Various DC voltages (0.5, 1, 1.5, 2, 2.5 V) were applied, and the current was measured for 1 h. The Keithley 2750 has an internal impedance of 10 GΩ in the voltage ranges utilized herein.[15] We, therefore, estimate the minimum measurable current to be 1 nA at 1 V (this corresponds to a resistance 10 times smaller than the internal impedance of the instrument). This low current corresponds to a conductivity of approximately 10^{-10} S cm^{-1} for our typical pellets with 5 mm diameters and thicknesses of about 0.4 mm. This is our estimate of the lowest measurable electronic conductivity for this instrument.

The gold contacts were then removed by sanding following the conductivity measurements, and the pellets were ground into powder. The powders were transferred into a high-throughput X-ray diffraction (XRD) holder where the samples lied on a thin mylar film. The XRD measurement of 64 samples required 10 h in transmission mode using a Panalytical goniometer equipped with a Mo X-ray source and a GaliPIX detector. The XRD data could be analyzed using either Rietveld or Pawley refinement methods as demonstrated in refs.[2, 12, 14]. The precision and reproducibility of the synthesis and XRD results have been shown to be excellent elsewhere.[13]

After XRD characterization, the powders were then transferred into stainless steel cups to prepare 64 electrode slurries for cycling to either a high or low potential for determining the stability window. Unlike our high-throughput studies on cathodes (e.g. refs.[11, 12, 14]) where a high loading was used to replicate industrial standards, we used here a low loading (approximately 1mg/cm^2) to ensure that poor transport within the electrode (that is composed of an insulating solid electrolyte) does not lead to overestimating the stability window. A PVDF and carbon black

solution was prepared in NMP. This solution was pipetted into 64 cups containing pre-weighed sample powders. Stirring for 15 min using a stir bar followed. The weight ratios (wt. %) of the electrode mixture SE:CB:PVDF were 84:11:5. Next, 3 μL of electrode slurry were pipetted onto each of the 64 pads of two printed circuit boards serving as current collectors in our high-throughput cells (Fig. 2). The first PCB had pads covered with gold to test the electrolytes' stability at low potentials and the other with aluminum for the high potential stability test. After drying the electrodes at 80 °C, the high-throughput electrochemical half-cell was assembled using two Whatman microfiber separators, liquid electrolyte (LE) which consists of 1M LiPF6 in EC/EMC = 3/7 (Soulbrain), and lithium foil. The electrochemical stability window test CVs were run on the same setup used for electronic conductivity measurement but with 1 kΩ resistors used to measure the current through each cell. The voltage was swept from 3 to 5.5 V for the high voltage (HV) test and from 3 to 0.1 V for the low voltage (LV) test at a sweeping rate of 0.1 V/h. Both cells were cycled for 1.5 cycles in order to be able to observe whether or not passivation occurred.

Importantly, all of the above could be performed on a single set of samples using the workflow proposed. In order to better identify the limitations of using carbonate-based electrolytes for these tests, a single sample of LLTO was also tested to high potential in a Swagelok cell using ionic liquid (IL) electrolyte (0.3 M bistrifluoromethanesulfonimide lithium salt from Sigma-Aldrich in 1-Butyl-1-methylpyrrolidinium bistrifluoromethanesulfonylimide ionic liquid from TCIchemicals). Finally, another batch of LLTO and LLZO samples was synthesized to test the chemical stability against lithium. Given the potential damage done by lithium contact and that this test required pellets, we saw no alternative but to prepare a second set when stability measurements vs. lithium were required. In this final test, one side of the pellets was sputtered with gold, and on the other side, a small disk of lithium foil was placed against the electrolyte.

Then, the EIS measurement was performed at different time intervals to track the interfacial impedance evolution using the previous EIS parameters.

Results & discussion

Ionic conductivity - Screening the ionic conductivity of solid electrolytes is essential because high ionic conductivity is essential to minimize the internal resistance of the cell. The ionic conductivity of a solid electrolyte is measured by electrochemical impedance spectroscopy (EIS). The total electrical conductivity of 64 similar composition LLTO samples was measured by EIS on a symmetric cell with gold ion blocking electrodes. Due to the negligible electronic conductivity of LLTO measured in the following electronic conductivity test, the electrical conductivity is considered to correspond to the ionic conductivity. The Nyquist plots of the 64 LLTO samples shown in Fig. 3 consist of two semicircle arcs and a tail at low, medium, and high frequencies, respectively. The EIS spectrum was fitted to an equivalent circuit consisting of two RC circuits in series with a capacitor (ref. [2, 13]). The capacitors were replaced by a constant phase element to model the non-ideal impedance response. The first semicircle arc is assigned to the bulk conductivity and the second to the grain boundary, while the tail corresponds to the polarization of the blocked ions at the SE/Au interface. The EIS measurements were performed at 22 °C and 50 °C, and the activation energy was extracted from the Arrhenius plot. The conductivities and activation energies obtained here and from the literature are given in table 1. The bulk and grain boundary conductivities of 64 LLTO samples obtained here are $(1.28 \pm 0.27) \times 10^{-3}$ S cm^{-1} and $(4.37 \pm 1.22) \times 10^{-5}$ S cm$^{-1,}$ respectively. Note: the uncertainties here are standard deviations such that they give a good indication of the variations to be expected in single sample measurements. We found standard deviations about 20 % or lower for conductivity values. Given that the objective in screening solid electrolytes is to obtain ionic conductivities above a certain threshold, this level

of precision is certainly sufficient. Furthermore, the activation energies were 0.28 eV for bulk conductivity and 0.37 eV for grain boundary conductivity. The activation energies are in excellent agreement with the literature values as shown in Table 1 while also showing very low standard deviations (0.02 eV at most) showcasing the high degree of reproducibility obtained in the activation energy measurements. Furthermore, for LLZO, a bulk conductivity of 1.36×10^{-6} S cm^{-1} was obtained with an activation energy of 0.51 eV, again in excellent agreement with the literature for this composition. These tests clearly show that the EIS setup is valid for a wide range of conductivity values as it has the reproducibility and precision necessary to effectively screen solid electrolytes. Furthermore, Fig. S1a shows the result for a single LLTO sample in a Swagelok style cell obtained at 4 different temperatures. The resulting values for activation energy are 0.30 eV (bulk) and 0.36 eV (grain), in good agreement with the result obtained in high-throughput at 2 temperatures only. We, therefore, feel this setup is optimal and effective for both RT ionic conductivities and near RT activation energies.

Electronic conductivity - The electronic contribution to the total electrical conductivity was measured by the DC polarization method. The electronic conductivity was calculated from the steady-state currents after applying different DC polarizations: 0.5, 1, 1.5, 2, and 2.5 V were applied to a symmetric Au/SE/Au cell, while the current was recorded for 60 min. As shown in Fig. 4a, the total current decreases due to the decay of the ionic current until it reaches a steady-state current, which corresponds to the electronic contribution to conductivity. Li/Se/Au cell configuration is not recommended for high-throughput studies because of the instability of some SE against lithium preventing its systematic use. The I-t plots of the Au/LLTO/Au cell under 2V is shown in Fig. 4 and S2. Clearly, the electronic conductivity lies well below the value of 2.2×10^{-9} S cm^{-1} where dendrite growth is a concern as discussed in the introduction, such that we can

conclude that dendrite growth will be greatly mitigated in LLTO, especially in comparison to LLZO that shows conductivities well above this value. Fig. 4 also shows the extracted electronic conductivities as a function of the applied voltages. The electronic conductivity of LLTO showed ohmic behavior between 0.5 V and 1.5 V, while the conductivities increased like a varistor at 2-2.5 V (Fig. 4b). The electronic conductivity measured for LLTO in the ohmic range is therefore (3 ± 2) × 10^{-10} S cm^{-1}. Again, this level of precision is excellent given that the required purpose is to determine if the electronic conductivity is below 3 × 10^{-9} S cm^{-1}. The value reported here is consistent with previous reports as shown in Table 1; importantly, the best agreement is found for reports where the measurements were performed in the Ohmic range.[16-18] To make sure the setup is versatile and able to measure electronic conductivities above the dendrite threshold, the electronic conductivity of the LLZO was determined. The electronic conductivity of LLZO was 1.28 × 10^{-7} S cm^{-1} at 1 V, in good agreement with what was found by Chen.[19] It is well known in the literature that electronic conductivity is a concern in garnet LLZO materials while not for perovskite electrolytes.[3] The fact that the high-throughput setup here dramatically shows this contrast confirms that this system will be effective in screening this important property for ceramic solid electrolytes.

Electrochemical stability window - Solid electrolytes should have a wide electrochemical stability window including the operation potentials of both electrodes. In our high-throughput methodology, the limits of the electrochemical stability window are determined by cyclic voltammetry of two cells. Working electrodes were prepared from the solid electrolytes by mixing them with carbon black to ensure sufficient electronic paths. Lithium half-cells were assembled using a liquid carbonate based electrolyte to ensure the ionic conduction does not limit current. Each sample was divided into two, one swept to 5.5 V and the other to 0.1 V as shown in Fig. 5.

In each cell, we alternated a row of blank cells (carbon black and PVDF only, in the same quantities as in the electrodes with electrolyte) with rows of LLTO and LLZO. The faradaic current of the solid electrolytes can then be compared to the blanks, and the point where the two diverge is identified as the end of the stability window. Fig. 5 clearly shows (as in refs. [11, 14]) that there is no cross-contamination between neighboring samples and the CVs of duplicates are highly reproducible. For the low voltage tests, the CVs of Li/LE/LLTO-C cells in Fig. 5a, 6a and S3a show a large reductive current (~4.0 μA) below 1.78 V, which is reversible and shows in the second cycle, indicating its instability (interphase propagation). This value is close to the theoretical value 1.75 V[20] also consistent with the previous experimental value of 1.8 V[21]. In contrast, the CV of Li/LE/LLZO-C at low voltages does not show reductive current compared to the carbon black indicating that it remains stable all the way down to 0.1 V. However, it must be acknowledged that determining the stability of SE at voltages close to zero is challenging because of the interference provided by the significant electrolyte degradation as the SEI builds. Thus, in cases where rigorous confirmation of low voltage stability is required, then a repetition of the test will be performed with a more stable liquid electrolyte (e.g., ionic liquid). We do not propose ionic liquid electrolytes for high-throughput screening given the high cost of ionic liquids, but we utilize it on occasion to confirm/refine high-throughput results (as illustrated below for the high voltage stability of LLTO). In the high voltage stability tests shown in Fig. 5b, 6b, S3b and S6 both LLTO and LLZO show small irreversible oxidative currents at 4.0 V (~0.5 μA), which do not appear on the second cycle and also appear in the blanks. The irreversibility could be caused by an irreversible process or the formation of a high impedance interphase. Fig. S3 shows clearly that LLZO exceeds the current of the blanks at 4.0 V and above, while LLTO does not exceed the blank at any voltage. Therefore, even in this case where electrolyte degradation interferes, we can establish the end of

the stability window of our solid electrolytes: 4.0 V for LLZO, while the LLTO appears to be stable over the entire range. As shown in table 1, this is in good agreement with the few reports of ESW in the literature that use a reliable method as discussed in the introduction. This oxidation limit determined for LLZO by the CV test is the same as the value obtained by Han[5] showing that our high-throughput stability test is consistent with the few appropriate results in the literature. However, for LLTO it is difficult to be conclusive about the stability window's upper limit given the interference by electrolyte degradation. Therefore, in Fig. S4 we repeat the measurements in ionic liquid electrolyte that shows very little degradation in the blanks. The result shows that the upper limit of the stability window for LLTO is in fact 4.7 V.[20] The higher experimental limits compared to the theoretical could be explained by the sluggish kinetic (overpotential).[5, 20] We therefore intend to use the test with the ionic liquid in cases where the solid electrolyte appears to be stable over the entire range (or as stable as the blank) in the high-throughput screening.

Chemical compatibility with lithium - Solid electrolytes can achieve high energy density when used with lithium metal anodes, so checking their compatibility is crucial. The stability of the SE against lithium was explored by measuring the EIS of asymmetric cell Li/Se/Au at different time intervals. Fig. 7a shows the impedance evolution of Li/LLTO/Au and Li/LLZO/Au cell with time. The total electrical conductivity of Li/LLTO/Au increased by time while the low-frequency tail, as shown in Fig. 7b disappeared, indicating the presence of electronic conductivity. This signifies the formation and propagation of a mixed conductor phase as was previously explored.[22] On the other hand, the total electrical conductivity of the Li/LLZO/Au decreased initially and later remained constant similar to others' observation[23] indicating stable interphase formation. These results are again consistent with the well-known trends in the literature that LLTO shows instability vs. Li metal while LLZO does not.[10, 22]

Conclusion

Although screening essential properties for solid electrolytes has emerged as a significant bottleneck in developing all-solid lithium batteries, no robust high-throughput methodology was previously reported for screening any property other than room temperature ionic conductivity. The tools introduced herein allow the high-throughput synthesis of solid electrolytes and screening various properties required for their integration into solid batteries. All methods are designed for sets of 64 samples and enable the fast automated testing of the ionic conductivity (2 h), activation energy (an extra 14 h), electronic conductivity (4 h to ensure we are in the Ohmic region), electrochemical stability window (2 cells running for 54 h) and the chemical stability against lithium (1 h per sample). The workflow is such that all tests (except lithium stability) can be performed on a single batch of samples in a 1-2 weeks time span). The stability against lithium is then to be utilized on a selection of samples that show promising stability at low potentials in the stability window test. The properties of two model materials LLTO and LLZO were measured in high-throughput using our infrastructure, and systematically the results showed excellent agreement with the literature, and produced small standard deviations thereby enabling effective and reproducible screening of these critical properties. The two materials were selected for their contrast in properties (e.g. the undoped LLZO showed a low ionic conductivity while the LLTO showed a much higher conductivity) such that the suite of methods has now been shown to be effective for materials over a wide range of properties' values. Furthermore, low standard deviations obtained for repeats of the same compositions systematically show that the high-throughput methods will have high precision in identifying materials with improved properties. This system is therefore now optimized to advance the development of novel solid electrolyte chemistries.

Supplemental Information

Supporting information associated with this paper includes Figures S1-S4.

Acknowledgments

This work was funded by a New Frontiers in Research Fund grant, by the Natural Sciences and Engineering Research Council of Canada under the auspices of a Discovery grant and by an FRQNT new researcher grant.

References

1. M. S. Beal, B. E. Hayden, T. Le Gall, C. E. Lee, X. Lu, M. Mirsaneh, C. Mormiche, D. Pasero, D. C. A. Smith, A. Weld, C. Yada and S. Yokoishi, *ACS Combinatorial Science*, **13**, 375 (2011).
2. A. Jonderian, M. Ting and E. McCalla, *Chemistry of Materials*, **33**, 4792 (2021).
3. A. Jonderian and E. McCalla, *Materials Advances*, **2**, 2846 (2021).
4. F. Han, A. S. Westover, J. Yue, X. Fan, F. Wang, M. Chi, D. N. Leonard, N. J. Dudney, H. Wang and C. Wang, *Nature Energy*, **4**, 187 (2019).
5. F. Han, Y. Zhu, X. He, Y. Mo and C. Wang, *Advanced Energy Materials*, **6**, 1501590 (2016).
6. T. Hakari, M. Nagao, A. Hayashi and M. Tatsumisago, *Journal of Power Sources*, **293**, 721 (2015).
7. T. Hakari, Y. Fujita, M. Deguchi, Y. Kawasaki, M. Otoyama, Y. Yoneda, A. Sakuda, M. Tatsumisago and A. Hayashi, *Advanced Functional Materials*, **32**, 2106174 (2022).
8. G. F. Dewald, S. Ohno, M. A. Kraft, R. Koerver, P. Till, N. M. Vargas-Barbosa, J. Janek and W. G. Zeier, *Chemistry of Materials*, **31**, 8328 (2019).
9. T. Swamy, X. Chen and Y.-M. Chiang, *Chemistry of Materials*, **31**, 707 (2019).
10. Y. Zhu, J. G. Connell, S. Tepavcevic, P. Zapol, R. Garcia-Mendez, N. J. Taylor, J. Sakamoto, B. J. Ingram, L. A. Curtiss, J. W. Freeland, D. D. Fong and N. M. Markovic, *Advanced Energy Materials*, **9**, 1803440 (2019).
11. T. Adhikari, A. Hebert, M. Adamič, J. Yao, K. Potts and E. McCalla, *ACS Combinatorial Science*, **22**, 311 (2020).
12. S. Jia, J. Counsell, M. Adamič, A. Jonderian and E. McCalla, *Journal of Materials Chemistry A*, **10**, 251 (2022).
13. E. McCalla, M. Parmaklis, S. Rehman, E. Anderson, S. Jia, A. Hebert, K. Potts, A. Jonderian, T. Adhikari and M. Adamič, *Canadian Journal of Chemistry*, **100**, 132 (2021).
14. K. P. Potts, E. Grignon and E. McCalla, *ACS Applied Energy Materials*, **2**, 8388 (2019).
15. Model 2750 Multimeter/Switch System User's Manual, in.
16. A. C. Sutorik, M. D. Green, C. Cooper, J. Wolfenstine and G. Gilde, *Journal of Materials Science*, **47**, 6992 (2012).
17. X. Cheng, J. Wang, W. Qiang and B. Huang, *Journal of the American Ceramic Society*, **103**, 3698 (2020).
18. J. Emery, J. Y. Buzare, O. Bohnke and J. L. Fourquet, *Solid State Ionics*, **99**, 41 (1997).
19. Y.-T. Chen, A. Jena, W. K. Pang, V. K. Peterson, H.-S. Sheu, H. Chang and R.-S. Liu, *The Journal of Physical Chemistry C*, **121**, 15565 (2017).
20. Y. Zhu, X. He and Y. Mo, *ACS Applied Materials & Interfaces*, **7**, 23685 (2015).
21. C. H. Chen and K. Amine, *Solid State Ionics*, **144**, 51 (2001).
22. Y. Inaguma, C. Liquan, M. Itoh, T. Nakamura, T. Uchida, H. Ikuta and M. Wakihara, *Solid State Communications*, **86**, 689 (1993).
23. A. Sharafi, S. Yu, M. Naguib, M. Lee, C. Ma, H. M. Meyer, J. Nanda, M. Chi, D. J. Siegel and J. Sakamoto, *Journal of Materials Chemistry A*, **5**, 13475 (2017).
24. A. Morata-Orrantia, S. García-Martín and M. Á. Alario-Franco, *Chemistry of Materials*, **15**, 3991 (2003).
25. J. Awaka, N. Kijima, H. Hayakawa and J. Akimoto, *Journal of Solid State Chemistry*, **182**, 2046 (2009).
26. F. Aguesse, J. M. López del Amo, V. Roddatis, A. Aguadero and J. A. Kilner, *Advanced Materials Interfaces*, **1**, 1300143 (2014).

Tables:

Table 1. Ionic conductivity, activation energy, electronic conductivity, and electrochemical stability window of LLTO and LLZO, all obtained using our high-throughput methods in this study and compared to results from traditional studies in the literature. The uncertainties on all values from this study are the standard deviations on the measurements and therefore represent the precisions of the high-throughput techniques developed here.

Parameter	LLTO		LLZO	
	This study	Literature	This study	Literature
σ_{bulk} (S cm^{-1})	$(1.28 \pm 0.27) \times 10^{-3}$	$(1.32 \pm 0.2) \times 10^{-3}$ (24)	1.36×10^{-6}	1.63×10^{-6} (25)
σ_{gb} (S cm^{-1})	$(4.37 \pm 1.22) \times 10^{-5}$	$5.01 \pm 0.3 \times 10^{-5}$ (24)	-----	-----
$E_{a,bulk}$ (eV)	0.27 ± 0.01	0.27 (26)	0.51	0.54 (25)
$E_{a,gb}$ (eV)	0.38 ± 0.02	0.36 (26)		
ESW (V)	1.78 – 4.7*	1.8 (21) – **	0 – 4	0 – 4 (5)
σ_e (S cm^{-1})	$(3 \pm 2) \times 10^{-10}$ (<1.5V) $(8 \pm 4) \times 10^{-10}$ (2V) $(32 \pm 4) \times 10^{-10}$ (2V)	5.59×10^{-10} (1-2V) (17)	1.28×10^{-7} (1V)	1.2×10^{-7} (0.1V) (19)

* difficult to identify upper limit as curve matches the blank. This limit was determined using a single sample with ionic liquid electrolyte (Figure S4).

** the upper limit of the window is not reported using a reliable method.

Figure captions:

Figure 1. High-throughput structural and electrochemical characterization tools for solid electrolyte discovery and screening. All measurements are performed on 64 samples at once and result in the properties shown in the radar plot: room temperature ionic conductivity (σ_{ionic}), activation energy (E_a), electronic conductivity ($\sigma_{electronic}$), stability at low voltage (LV) and high voltage (HV). Each measurement is shown in greater detail throughout this manuscript.

Figure 2. The scheme of the high-throughput synthesis and structural/chemical/electrochemical characterization of solid electrolytes. Precursors are first dispensed into 64 alumina cups, then preheated with an aluminum plate to prevent mixing, samples are then pelletized in high-throughput, sintered to high temperature on alumina plates. Prior to conductivity tests, pellets are coated with gold, then assembled in the house-made cell with spring mounted contacts. After conductivity measurements, samples are crushed into powders and XRD is performed. Finally, the powders are mixed into slurries to make electrodes for the electrochemical stability tests on aluminum for HV, and on gold for LV.

Figure 3. Nyquist plots of identical LLTO samples measured on Au/LLTO/Au cell using EIS at (a) 22 °C, and (b) 50 °C. The red lines are the fits to the equivalent circuit. From the fits, ionic conductivity and activation energy are extracted and presented in Table I.

Figure 4. (a) DC polarization curves for 64 identical LLTO samples and a single LLZO sample (inset) measured in Au/SE/Au cell configuration. (b) The average steady state current (I_e) for the LLTO samples vs the applied DC voltage. The inset is a zoom-in on the Ohmic region.

Figure 5. (a) CV profiles of identical LLTO samples (blue), LLZO samples (red) and blank (carbon black and PVDF only, black) swept from 3 V down to 0.1 V at 0.1 V/h scan rate. The solid

electrolytes were made into electrodes as described in the text for this electrochemical stability window test. (b) CV profiles from 3-5.5 V at 0.1 V/h scan rate in a half cell configuration with the solid electrolytes made into electrodes for electrochemical stability window test. Both sets of CVs were run for 1.5 cycles.

Figure 6. Electrochemical stability of LLTO and LLZO at low and high voltage from Figure 5, overlayed for comparison. The CVs of same composition LLTO, LLZO, and blank cycled as cathodes shows the accuracy of the tool. The arrow indicates the feature that appeared on the first cycle. The stability windows in Table I were extracted from this data.

Figure 7. The EIS spectra evolution as a function of time after contact with lithium. The Nyquist plots are shown for LLTO (a) and LLZO (b) in the asymmetric configuration Li/SE/Au.

Figures

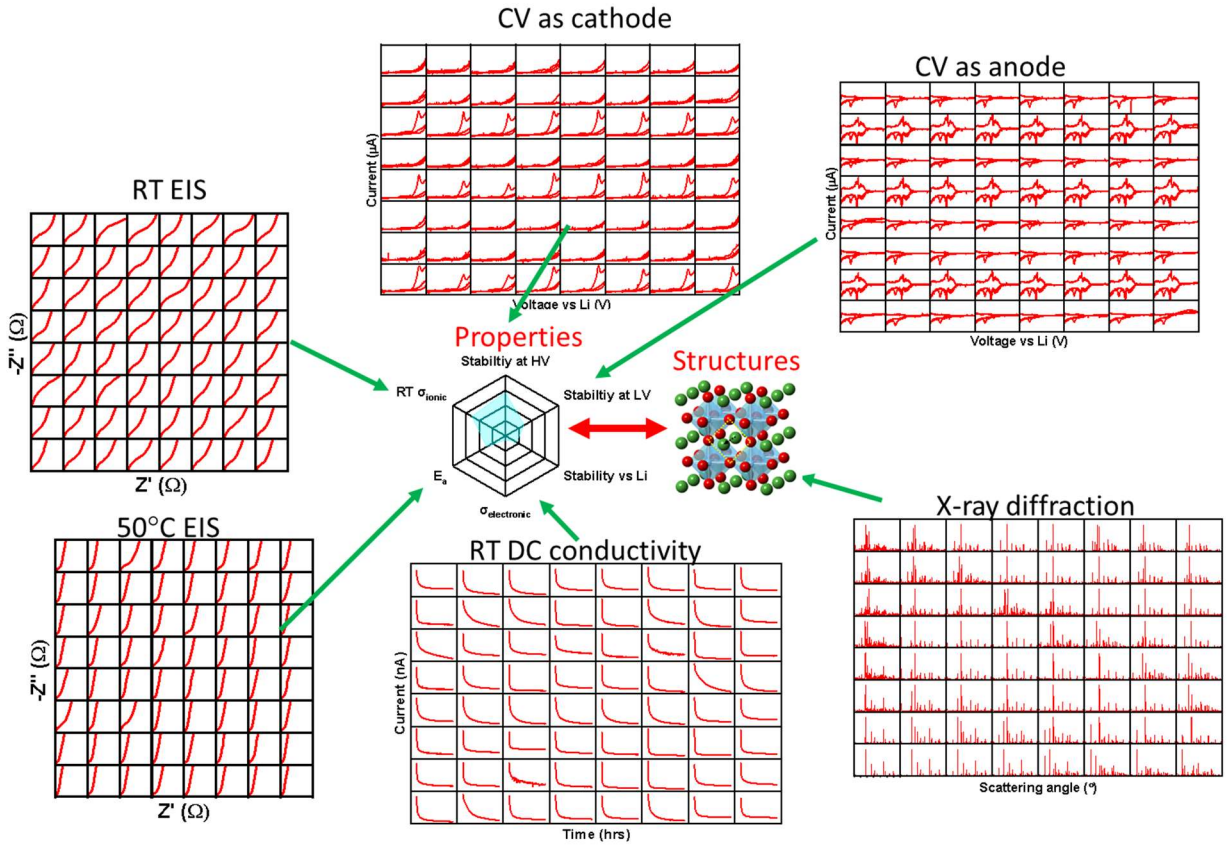

Figure 1.

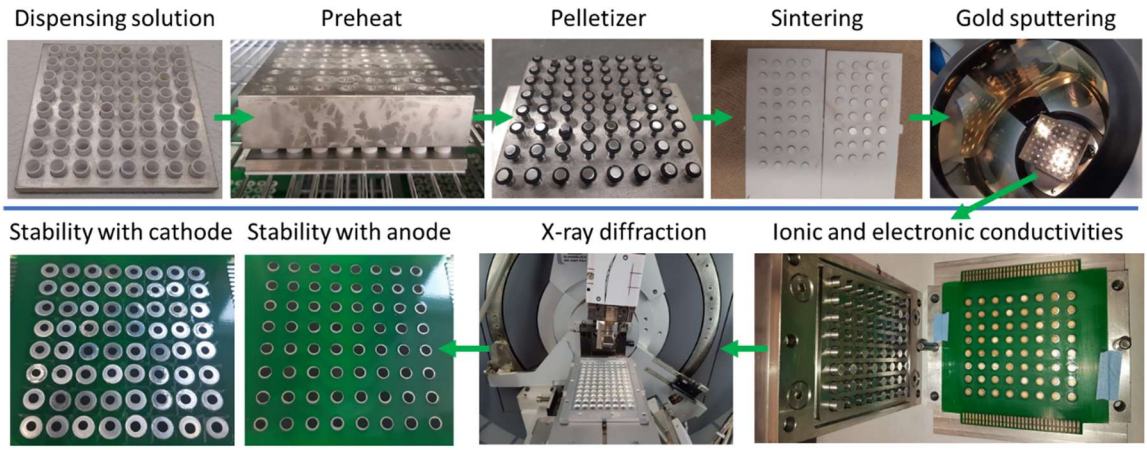
Dispensing solution
Preheat
Pelletizer
Sintering
Gold sputtering
Stability with cathode
Stability with anode
X-ray diffraction
Ionic and electronic conductivities

Figure 2.

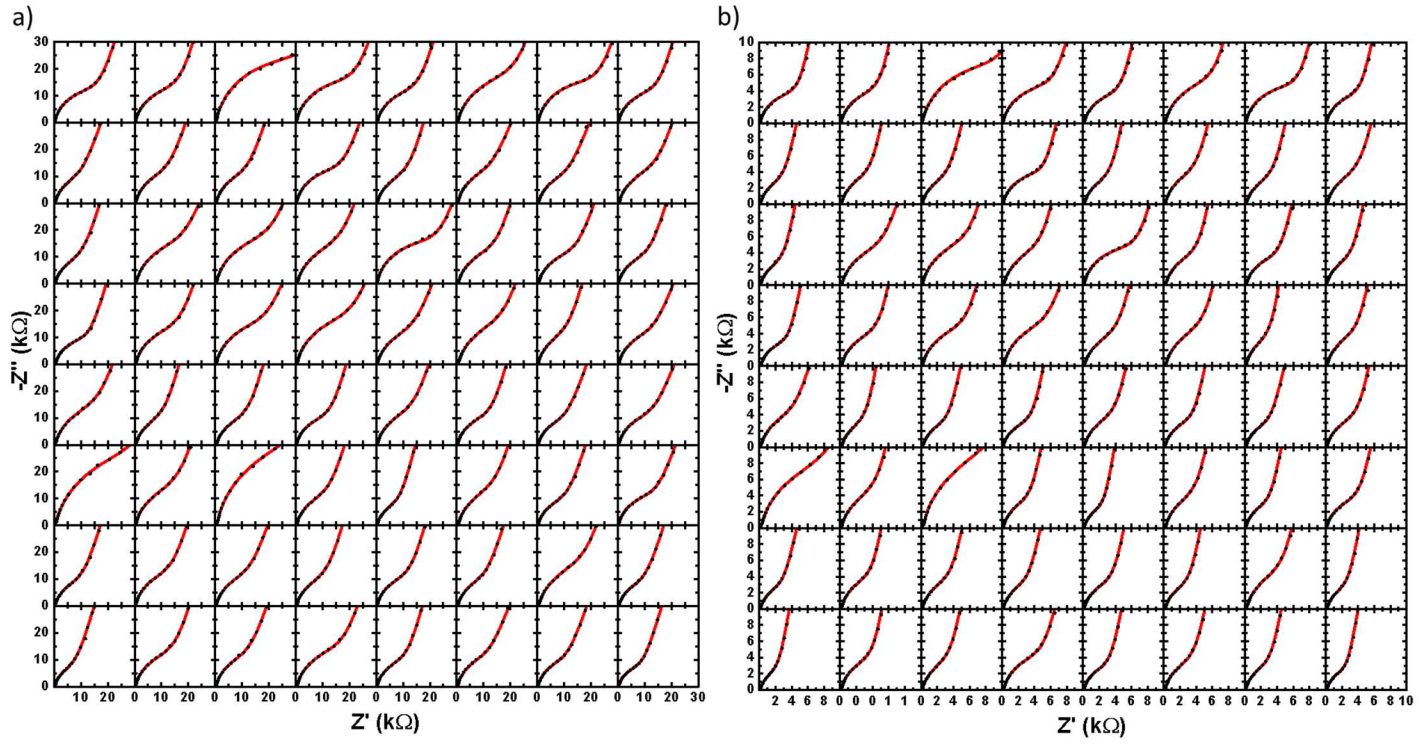

Figure 3.

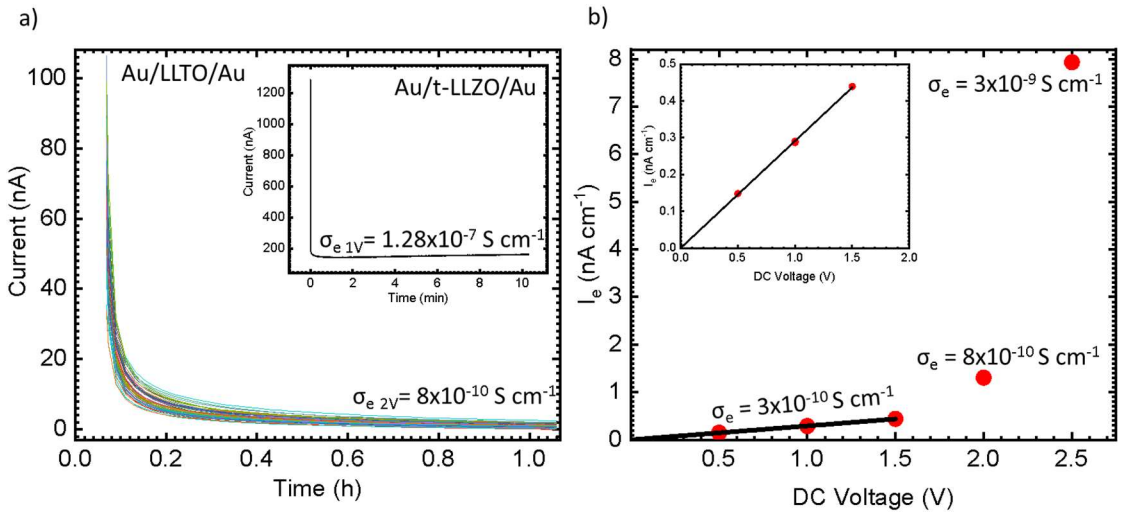
a)
Au/LLTO/Au
Au/t-LLZO/Au
Current (nA)
Time (h)
Time (min)
σe 1V= 1.28x10-7 S cm-1
σe 2V= 8x10-10 S cm-1
b)
Ie (nA cm-1)
DC Voltage (V)
σe = 3x10-9 S cm-1
σe = 8x10-10 S cm-1
σe = 3x10-10 S cm-1

Figure 4.

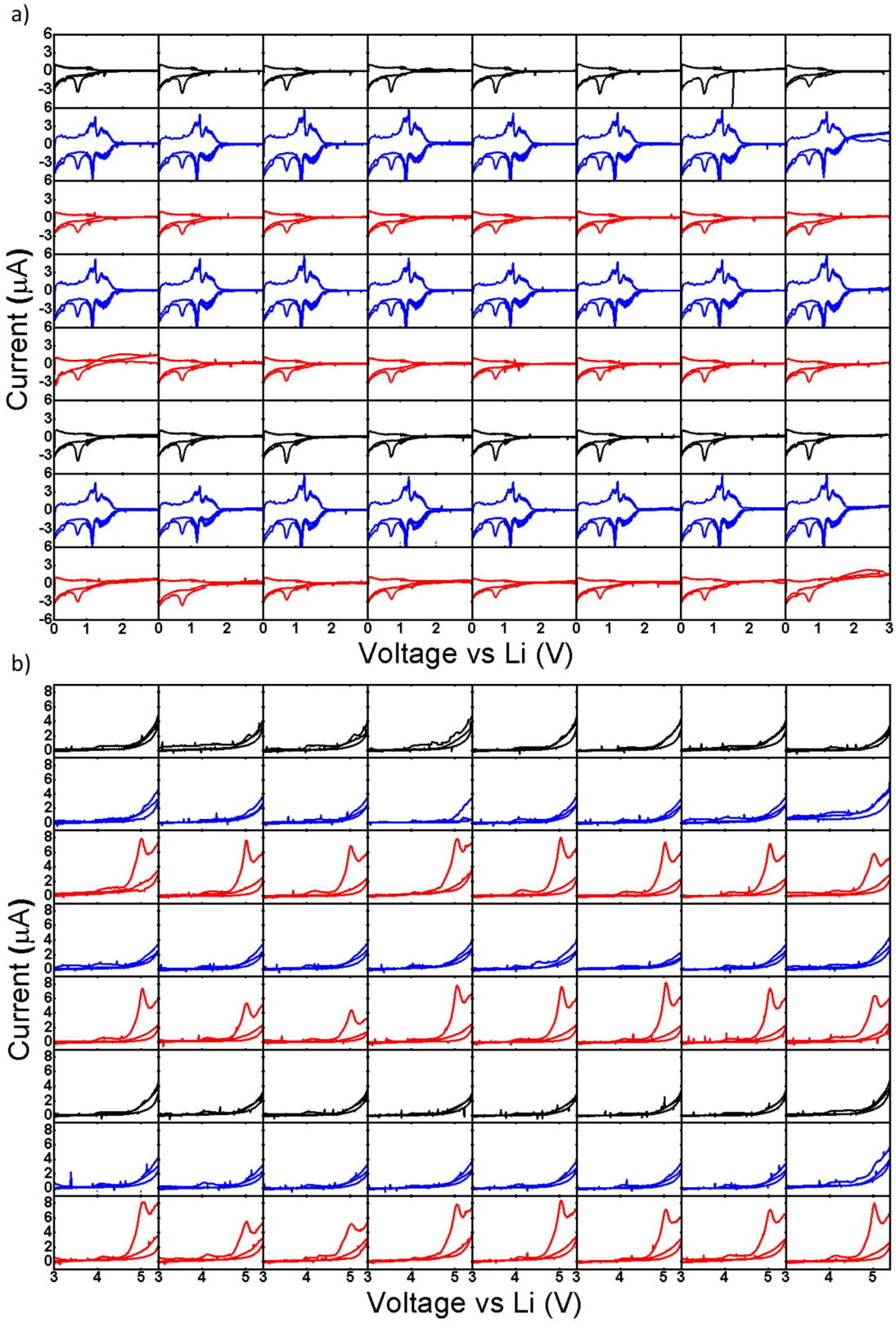

Figure 5.

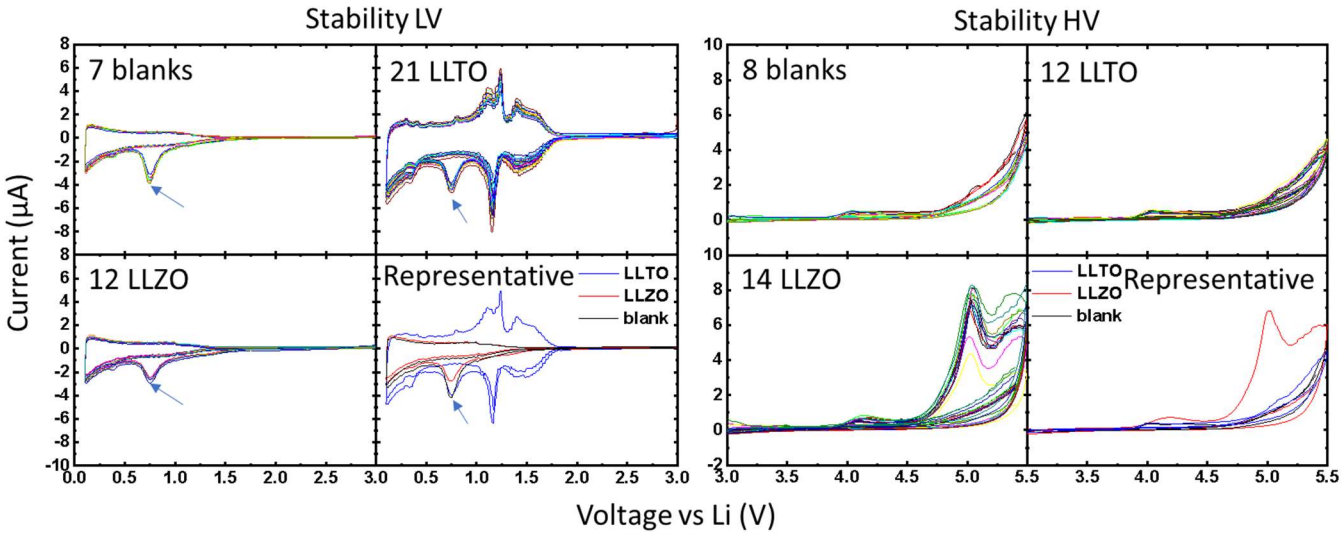
Stability LV
Stability HV
7 blanks
21 LLTO
8 blanks
12 LLTO
12 LLZO
Representative
14 LLZO
Representative
LLTO
LLZO
blank
Current (μA)
Voltage vs Li (V)

Figure 6.

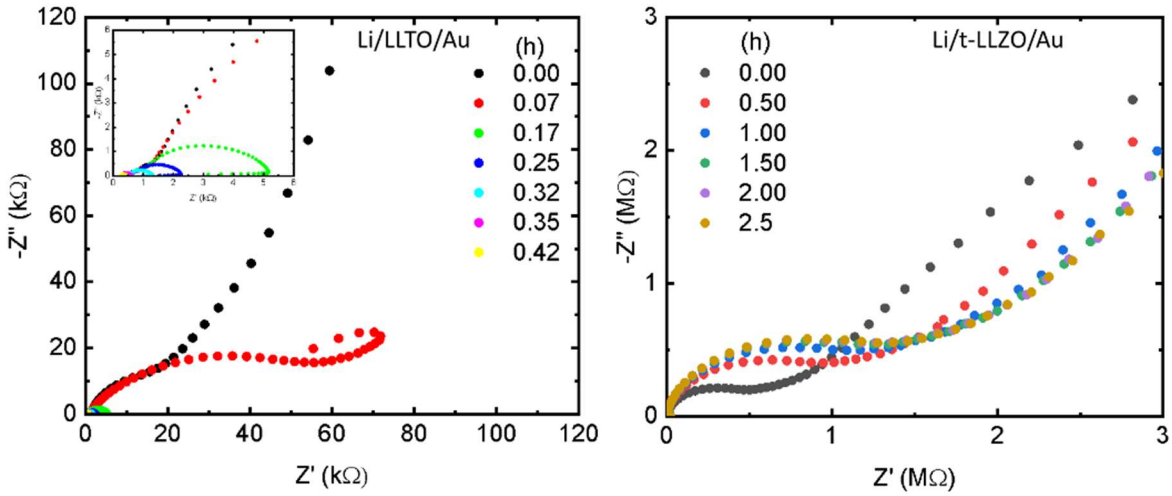
Li/LLTO/Au
(h)
0.00
0.07
0.17
0.25
0.32
0.35
0.42
-Z'' (kΩ)
Z' (kΩ)
Li/t-LLZO/Au
(h)
0.00
0.50
1.00
1.50
2.00
2.5
-Z'' (MΩ)
Z' (MΩ)

Figure 7.